Supporting information for

Deep-red light-up signaling of benzo[*c,d*]indole-quinoline monomethine cyanine for imaging of nucleolar RNA in living cells and for sequence-selective RNA analysis

Yukina Yoshino, Yusuke Sato,* and Seiichi Nishizawa*

Department of Chemistry, Graduate School of Science, Tohoku University, Japan, Sendai 980-8578, Japan.

*Corresponding authors: E-mail: yusuke.sato.a7@tohoku.ac.jp Telephone: +81 22 795 6551; E-mail: seiichi.nishizawa.c8@tohoku.ac.jp Telephone: +81 22 795 6549

Contents

1. Synthesis of BIQ and PNA-BIQ (Scheme S1, Figs. S1-S4)
2. pH effect on the absorbance and emission spectra of BIQ (Fig. S5)
3. Absorbance spectral change of BIQ upon binding to nucleic acids (Fig. S6)
4. Photostability of BIQ (Fig. S7)
5. Response of BIQ for synthetic nucleic acids and other biomolecules (Figs. S8 and S10)
6. CD spectra of rG and dG in the absence and presence of BIQ (Fig. S9)
7. Co-staining of the living cells with BIQ and organelle-selective staining agents (Fig. S11)
8. Co-staining of the fixed-permeabilized cells with BIQ and Hoechst 33342 (Fig. S12)
9. Co-staining of the live cells with BIQ and SYTO RNA select (Fig. S13)
10. Binding affinity of BIQ and SYTO RNA select for rG/rC (Fig. S14)
11. Evaluation of cytotoxicity of BIQ (Figs. S15 and S17)
12. Fluorescence images of the living cells incubated with 0.1-5.0 μM BIQ for 24 h (Fig. S16)
13. Fluorescence images of the living cells with the no-wash protocol (Fig. S18)
14. Fluorescence response of PNA-BIQ for the fully-matched dsRNA at pH 5.5 or pH 7.0 (Fig. S19)
15. UV spectra of PNA-BIQ for the fully-matched dsRNA (Fig. S20)
16. Binding affinity of PNA-BIQ for the fully-matched dsDNA (Fig. S21)
17. Effect of the base pair opposite the BIQ unit (Fig. S22)
18. Fluorescence quantum yield of PNA-BIQ, PNA-QB, and PNA-TO (Table S1)
19. Fluorescence response of PNA-BIQ for target ssRNAs (Fig. S23)
20. Time-dependent fluorescence change of the probes for RNAs (Fig. S24)

Synthesis of BIQ:

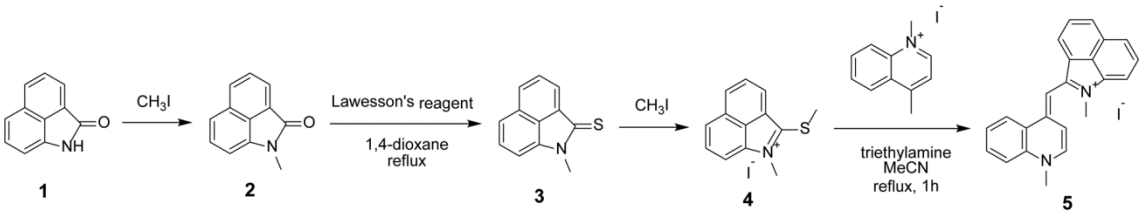

Scheme S1. Synthetic scheme for the preparation of BIQ.

1-methylbenzo[*c,d*]indol-2(1H)-one (2):[S1] Benzo[*c,d*]indol-2(1H)-one (1) (1.68 g, 9.93 mmol) and potassium carbonate (2.74 g, 19.8 mmol) were dissolved in DMF (30 mL). After the dropwise addition of methyl iodide (1.67 g, 11.8 mmol), the mixed solution was stirred at 38˚C for 2 days. The reaction mixture was extracted with ethyl acetate (75 mL × 2). The organic layer was washed with brine and dried over Na_2SO_4. The solid was filtered off, and the filtrate was concentrated under reduced pressure. The resulting crude product was purified by silica gel chromatography with chloroform to yield the purified **2** as a yellow solid (1.14 g, 63%).

^{1}H-NMR (500 MHz, DMSO-d_6): δ = 8.17 (d, J = 8.2 Hz, 1H), 8.04 (d, J = 6.7 Hz, 1H), 7.79 (dd, J = 7.9, 7.0 Hz, 1H),7.63 (d, J = 8.2 Hz, 1H), 7.55 (dd, J = 8.2, 7.0 Hz, 1H),7.16 (d, J = 7.0 Hz, 1H), 3.37 (s, 3H).

1-methylbenzo[*c,d*]indol-2(1H)-thione (3): 1-methylbenzo[*c,d*]indol-2(1*H*)-one (**2**) (0.55 g, 3.0 mmol) and Lawesson's reagent (2.43 g, 6.0 mmol) were dissolved in 1,4-dioxane (40 mL). The reaction mixture was stirred at 100 °C overnight. After cooling to room temperature, the solid was collected by filtration and washed with 1,4-dioxane. This affords the crude **3**, verified by ESI-MS.

1-methyl-2-(methylthio) benzo[*c,d*]indole-1-ium (4) (ref 9a in the main text): A mixture of the crude compound **3** (1.71 g) and iodomethane (20 mL) was heated to reflux overnight. After removing iodomethane in vacuo, the resulting residue was treated with diethyl ether (60 mL), followed by sonication for 30 min. The solid was collected by filtration to yield the crude **4**, verified by ESI-MS. This was used for next step without further purification.

(*E*)-1-methyl-2-((1-methylquinolin-4(1H)-ylidene)methyl)benzo[*c,d*]indol-1-ium iodide (5, BIQ): The crude compound **4** (194 mg, 0.57 mmol) dissolved in 12 mL of CH_3CN, was mixed with

1,4-dimethylquinolin-1-ium iodide (258 mg, 0.91 mmol) and TEA (0.5 mL). The mixture was refluxed for 1h. Upon cooling to room temperature, diethyl ether was added. The solid was collected by filtration and washed with deionized water. After the obtained solid was dissolved in methanol, diethyl ether was added. This affords **5** as a blue solid (82.2 mg, 32%).

^{1}H-NMR (700 MHz, DMSO-d_6): δ = 8.87 (d, J = 4.7 Hz, 1H), 8.75 (d, J = 7.3 Hz, 1H), 8.62 (br, 1H), 8.48 (br, 1H), 8.30 (d, J = 9.0 Hz, 1H), 8.17 (t, J = 7.3 Hz, 1H), 8.04 (d, J = 7.7 Hz, 1H), 7.92 (t, J = 7.5 Hz, 1H), 7.54 (m, 3H), 7.21 (br, 1H), 6.79 (br, 1H), 4.40 (s, 3H), 3.73 (s, 3H); ^{13}C-NMR (176 MHz, DMSO-d_6): δ = 152.84, 151.92, 146.73, 142.85, 138.78, 134.43, 129.98, 129.74, 129.46, 128.81, 128.29, 126.72, 126.05, 122.71, 119.37, 118.90, 115.90, 105.08, 95.69, 43.72, 30.37; ESI-MS for $C_{23}H_{19}N_2$ ($[M]^+$): calcd, 323.15; found, 323.17.

(A)

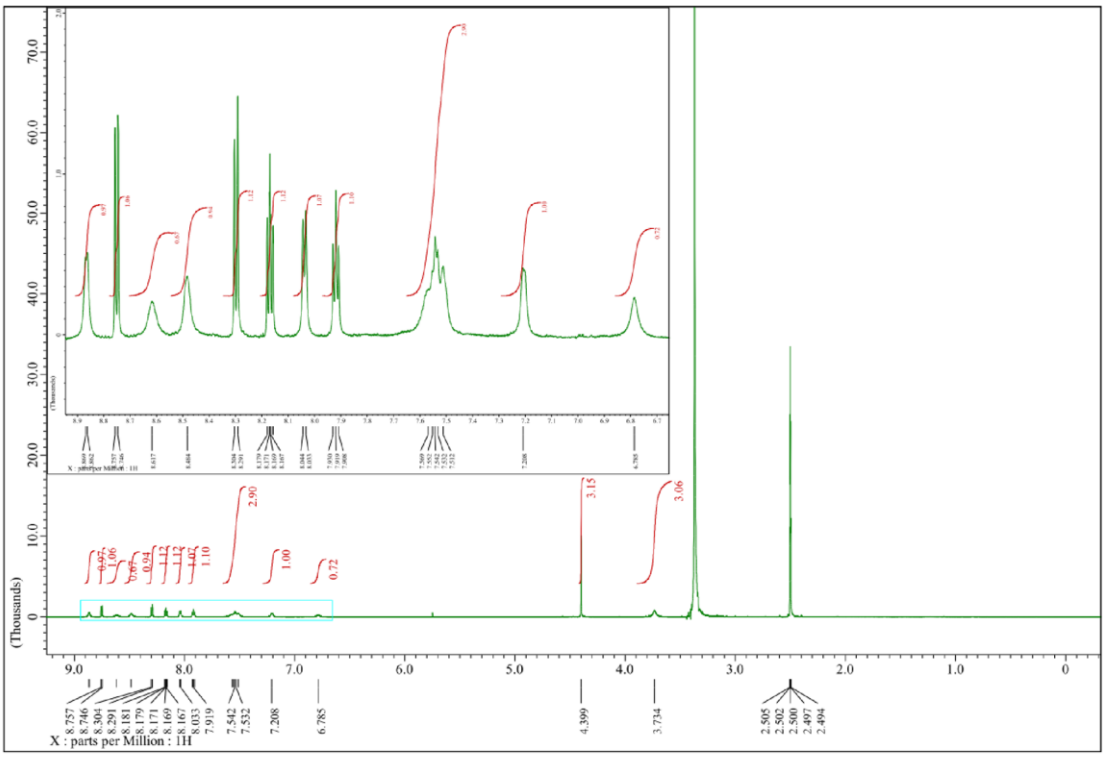

(B)

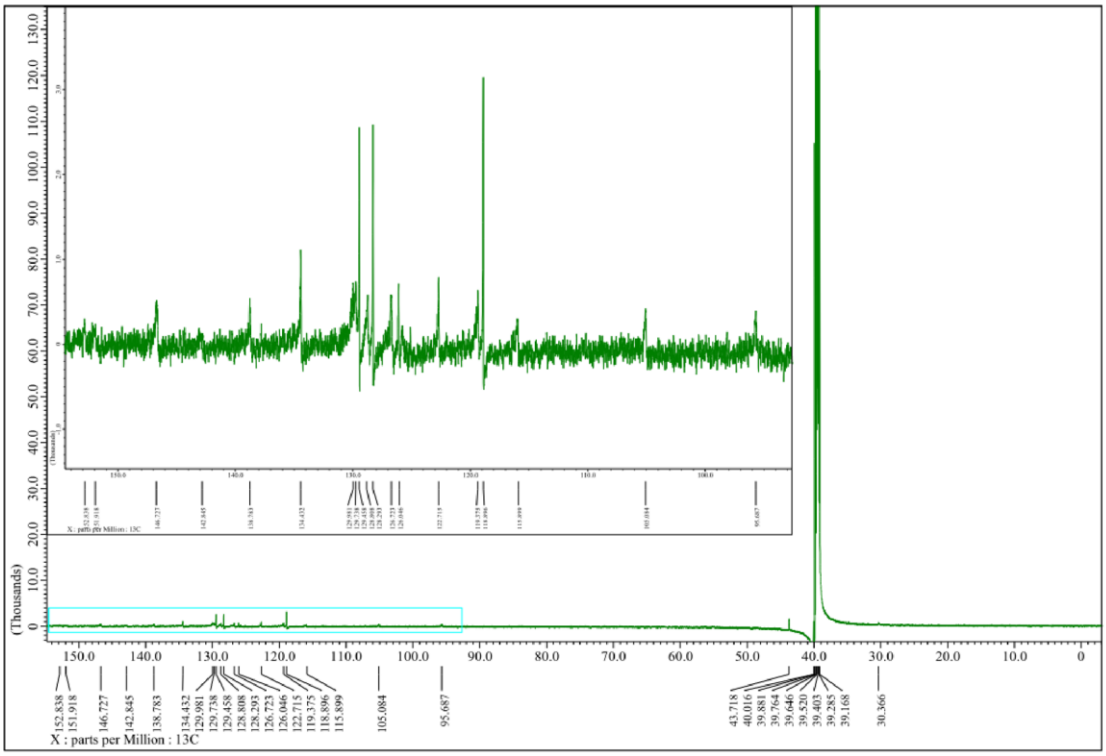

Figure S1. (A) ^{1}H NMR and (B) ^{13}C NMR spectra of BIQ in DMSO-d_6.

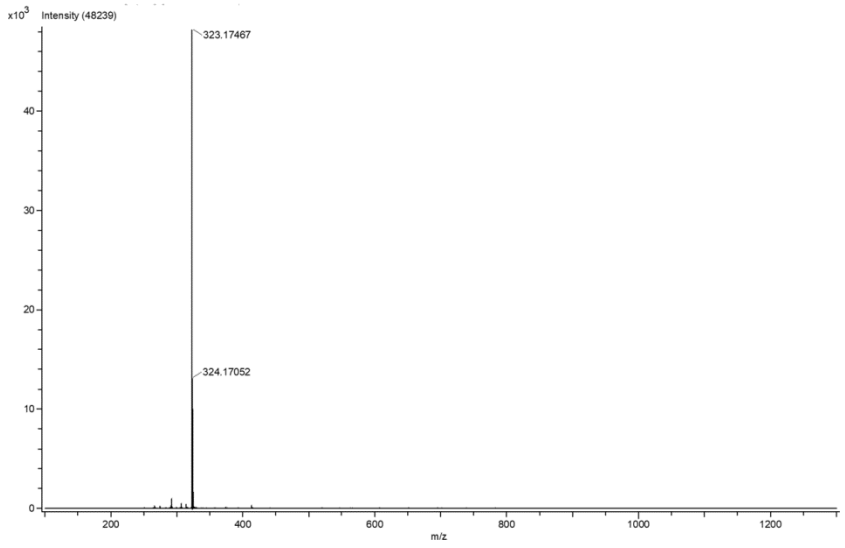

Figure S2. ESI-MS spectrum of BIQ.

Synthesis of PNA-BIQ: PNA-BIQ was synthesized by solid phase synthesis based on Fmoc/Bhoc chemistry, with a Rink-Amide-Chem Matrix resin. The assembly on the resin was performed by repetitive cycle of Fmoc deprotection with 20% piperidine in DMF (2 × 1 min) and 5% DBU (2 × 1 min), coupling with COMU/DIEA in NMP (2 × 10 min) in a microwave reactor (Biotage Initiator, Biotage, Uppsala, Sweden), and capping with 5% acetic anhydride/6% lutidine in DMF (2 × 1 min). The completion of coupling reactions was checked by the Kaiser test. Fmoc-aeg(alloc)-OH was utilized for introducing the BIQ base surrogate. After completion of the elongation of all monomer units, the alloc group was selectively deprotected with 8 equimolar diethylamine borane and an equimolar tetrakis(triphenylphosphine) palladium (0) in dichloromethane (2 × 45 min). Then, carboxylated BIQ, obtained by reacting 1-carboxymethyl-4-methylquinolium bromide[S2] with crude **4** according to the same procedure for BIQ (**5**) synthesis, was coupled with the resulting free secondary amine by using TOTU/PPTS/DIEA (2 × 24 h). After deprotection of the terminal Fmoc group, deprotection of Bhoc groups in the PNA nucleotides and cleavage from the resin were carried out using a mixture of trifluoroacetic acid (TFA)/*m*-cresol (85/15). The solution was dropped into cold diethyl ether in order to participate the crude product. The crude product was purified by a reverse-phase HPLC system (pump, PU-2086 Plus ×2; mixer, MX 2080-32; column oven, CO-1565;

detector, UV-2070 plus and UV-1570M (Japan Spectroscopic Co. Ltd., Tokyo, Japan)) equipped with a C18 column (Inertsil ODS3; GL Sciences Inc., Tokyo, Japan) using a gradient of water/acetonitrile containing 0.2% TFA (Fig. S3). PNA-BIQ was verified by MADLI-TOF-MS, as shown in Fig. S4 (4800 Plus MALDI TOF/ TOF analyzer: AB Sciex, Tokyo, Japan).

The concentration of PNA-BIQ was determined by measuring the absorbance at 260 nm in MilliQ water. The extinction coefficients at 260 nm (ε_{260}) for thymine and cytosine in the probe were 8800 $M^{-1}cm^{-1}$ and 7300 $M^{-1}cm^{-1}$, respectively. ε_{260} value of BIQ unit was assumed to be the same as that of adenine (ε_{260} = 13700 $M^{-1}cm^{-1}$).

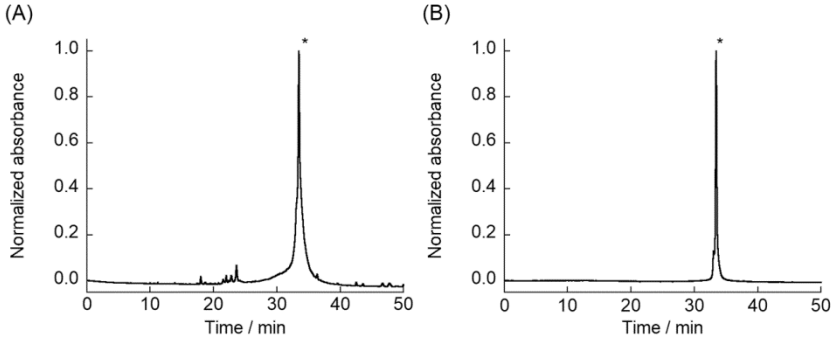

Figure S3. HPLC profile for the purification of PNA-BIQ. Gradient condition: 10-45% CH_3CN (0.2% TFA) in H_2O (0.2% TFA) during 50 min. Absorbance (A) at 260 nm for PNA unit and (B) at 600 nm for BIQ unit was monitored. The peak (*, retention time = 33.5 min) was collected and identified as the purified PNA-BIQ by MALDI-TOF-MS (cf. Fig. S4).

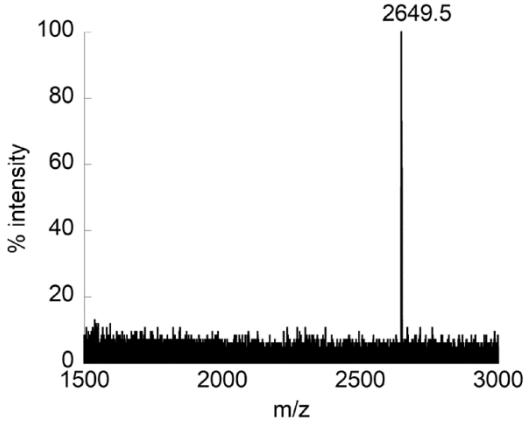

Figure S4. MALDI-TOF-MS spectrum of the purified PNA-BIQ.

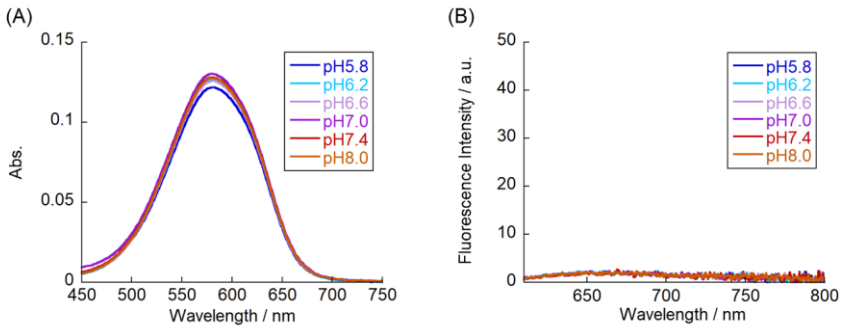

Fig. S5. (A) Absorption and (B) emission spectra of BIQ (5.0 μM) at various pH values from pH 5.8 and pH 8.0. Measurements were done in a 10 mM sodium phosphate buffer.

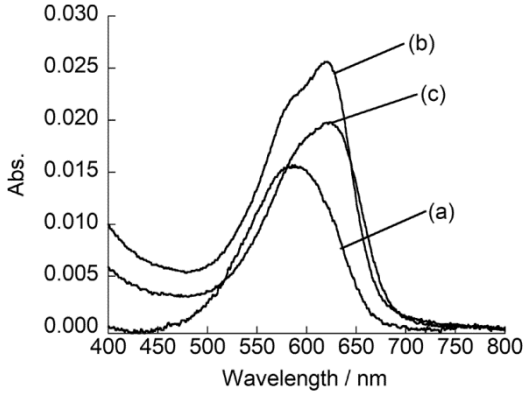

Figure S6. Absorption spectra of BIQ (1.0 μM) in the (a) absence and presence of (b) 1.0 mM *E.coli* total RNA or (c) 1.0 mM calf thymus DNA. Other solution conditions were the same as those given in Fig. 1B. Temperature, 25°C.

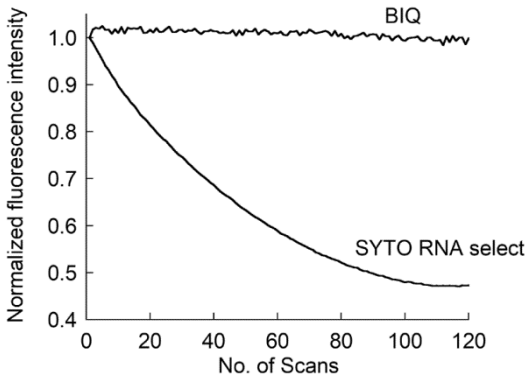

Figure S7. Decrease in the fluorescence intensity of BIQ bound to *E. coli* total RNA under continuous irradiation for 120 scans. The results for SYTO RNA select were also shown. [BIQ] = 1.0 μM, [SYTO RNA select] = 1.0 μM, [*E. coli* total RNA] = 1.0 mM. Measurement was done after mixing BIQ and RNA solutions and subsequent incubation for 30 min. Other solution conditions were the same as those given in Fig. 1B in the main text. Excitation: 595 nm (BIQ), 490 nm (SYTO RNA select). Analysis: 657 nm (BIQ), 530 nm (SYTO RNA select). Temperature, 25°C.

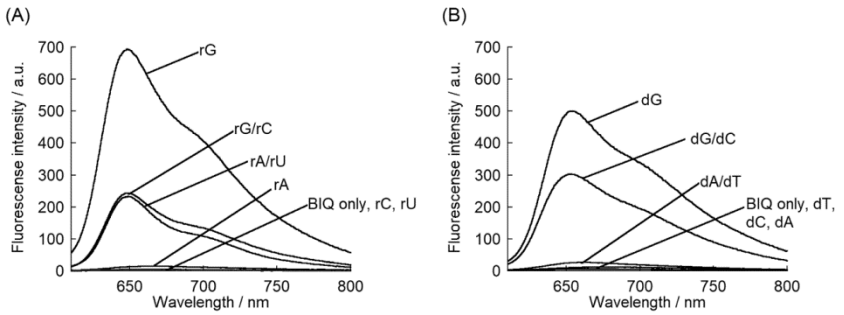

rG: 5' -r(GGG GGG GGG GGG G)-3'
rC: 5' -r(CCC CCC CCC CCC C)-3'
rA: 5' -r(AAA AAA AAA AAA A)-3'
rU: 5' -r(UUU UUU UUU UUU U)-3'

dG: 5' -d(GGG GGG GGG GGG G)-3'
dC: 5' -d(CCC CCC CCC CCC C)-3'
dA: 5' -d(AAA AAA AAA AAA A)-3'
dT: 5' -d(TTT TTT TTT TTT T)-3'

Figure S8. Fluorescence response of BIQ (5.0 μM) for synthetic nucleic acids (20 μM: (A) RNA and (B) DNA). Excitation, 595 nm. Temperature, 25°C. RNA and DNA sequences used here were also shown.

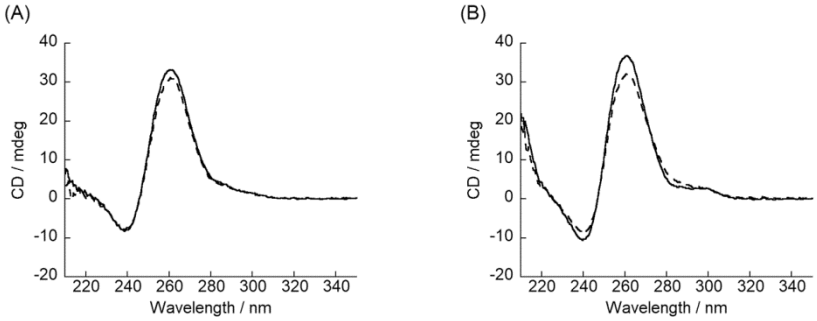

Figure S9. CD spectra of (A) rG and (B) dG in the absence (solid line) and presence of BIQ. [rG], [dG] = 5.0 μM. [BIQ] = 5.0 μM. Other solution conditions were the same as those given in Fig. 1B in the main text.

We observed the pronounced positive signal at 260 nm and the negative peak at 240 nm in the CD spectra of both rG and dG, which indicates the formation of parallel G-quadruplex.[S3] The addition of BIQ caused little change in the CD spectra, which indicates the resulting complex remains in the G-quadruplex structure without any drastic conformational change. Thus, the observed light-up response of BIQ for these sequences would arise from the binding to the G-quadruplex structure.

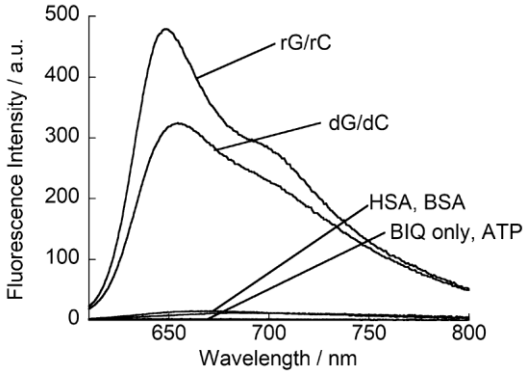

Figure S10. Fluorescence response of BIQ (5.0 μM) for other biomolecules (20 μM: human serum albumin (HSA), bovine serum albumin (BSA) and adenosine triphosphate (ATP)). Excitation, 595 nm. Temperature, 25°C. Other solution conditions were the same as those given in Fig. 1B in the main text.

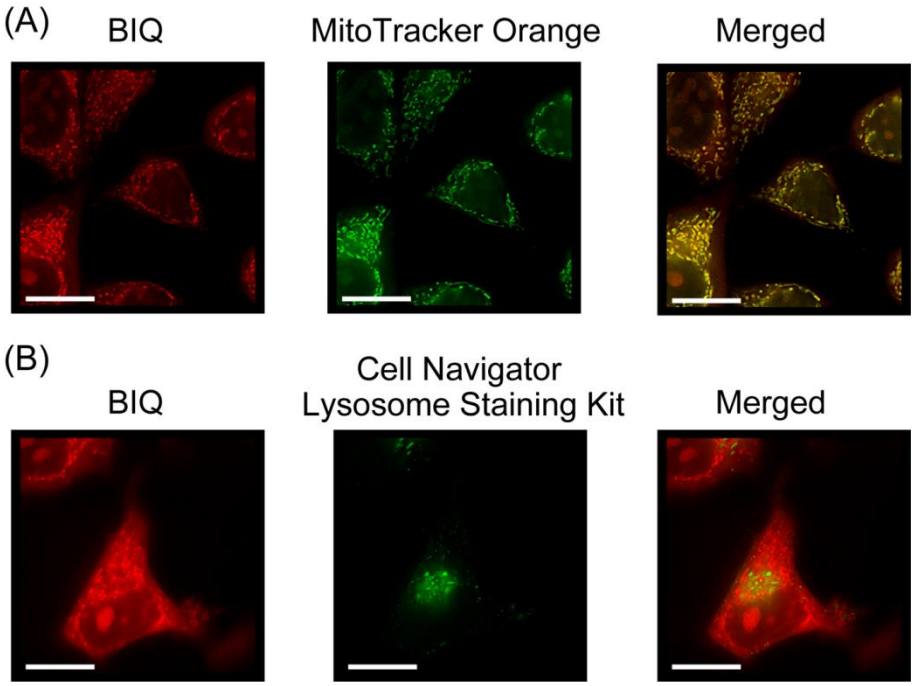

Figure S11. Co-staining of live MCF7 cells with BIQ and (A) MitoTracker Orange or (B) Cell Navigator Lysosome Staining Kit in the living MCF-7 cells. [BIQ] = 5.0 μM, [MitoTracker Orange] = 100 nM. [Cell Navigator Lysosome Staining Kit] = 100 nM. Scale bar: 15 μm.

The fluorescence of BIQ in the cytoplasma was well overlapped with that of MitoTracker Orange (Pearson's correlation coefficient: 0.88), which indicates that BIQ is accumulated in the mitochondria.

Figure S12. Co-staining of fixed-permeabilized MCF7 cells with BIQ and Hoechst 33342. [BIQ] = 5.0 μM. [Hoechst 33342] = 176 nM. Scale bar: 15 μm.

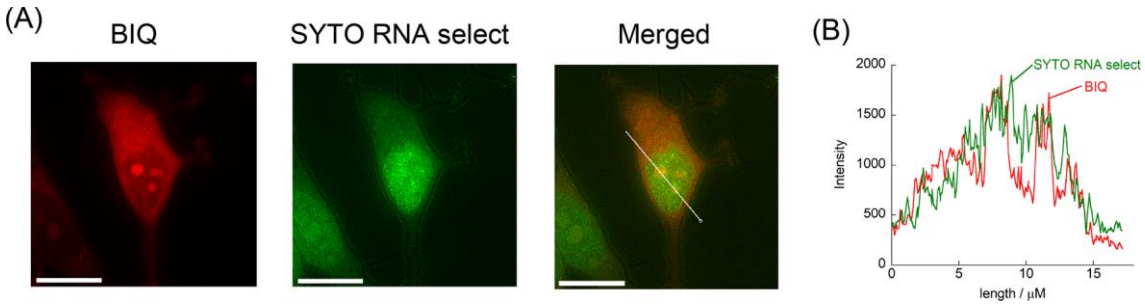

Figure S13. (A) Co-staining of live MCF7 cells with BIQ and SYTO RNA select. [BIQ] = 5.0 μM, [SYTO RNA select] = 0.5 μM. Scale bar: 15 μm. (B) Fluorescence intensity profile along the white line in the merged image in Fig. S13A.

As clearly seen in the fluorescence intensity profiles, BIQ had the better imaging selectivity for the nucleolus over the nucleus compared to SYTO RNA select.

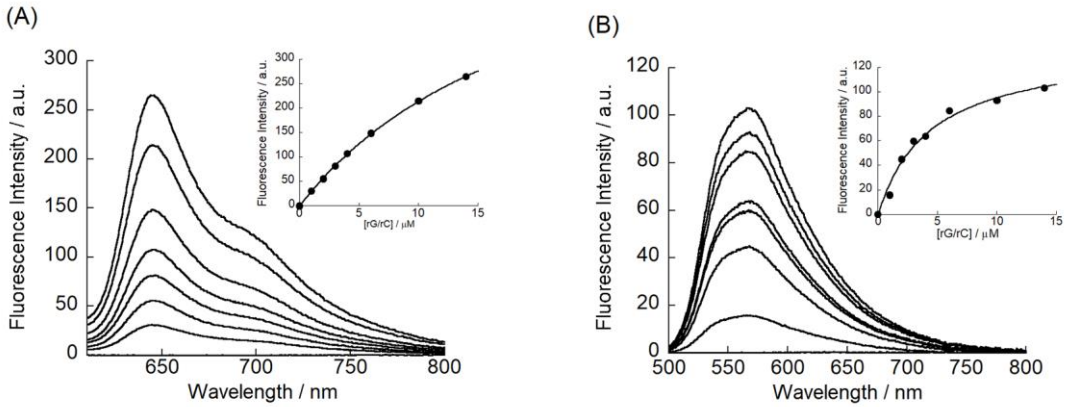

Figure S14. Fluorescence titration curve for the binding of (A) BIQ and (B) SYTO RNA select for rG/rC. [probe] = 1.0 μM. [rG/rC] = 0-14 μM. Other solution conditions were the same as those given in Fig. 1B in the main text. Excitation: 595 nm (BIQ); 490 nm (SYTO RNA select). Analysis: 645 nm (BIQ); 567.5 nm (SYTO RNA select). Temperature, 25°C.

Both probes showed the light-up response upon binding to rG/rC and its response was concentration-dependent. As for SYTO RNA select, the apparent dissociation constants (K_d) was estimated as 3.4 ± 1.2 μM (N = 3) by the analysis of the titration curve based on a 1:1 binding model.[S4] On the other hand, the titration curve for BIQ did not saturate under the identical condition (K_d > 22 μM). Even in the titration curve with higher BIQ (5 μM) and rG/rC (0-32 μM) concentration, we did not observe the binding saturation due to the weak affinity. This may be also due to the increased stoichiometry for the BIQ binding. From these results, the binding affinity of BIQ should be weaker by at least 10-fold relative to that of SYTO RNA select.

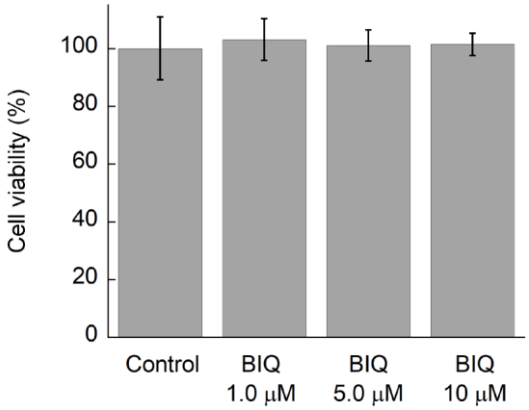

Figure S15. Evaluation of cytotoxicity of BIQ after 20 min incubation. Buffer treatment served as a positive control. Error bars represent standard deviation obtained from three independent experiments.

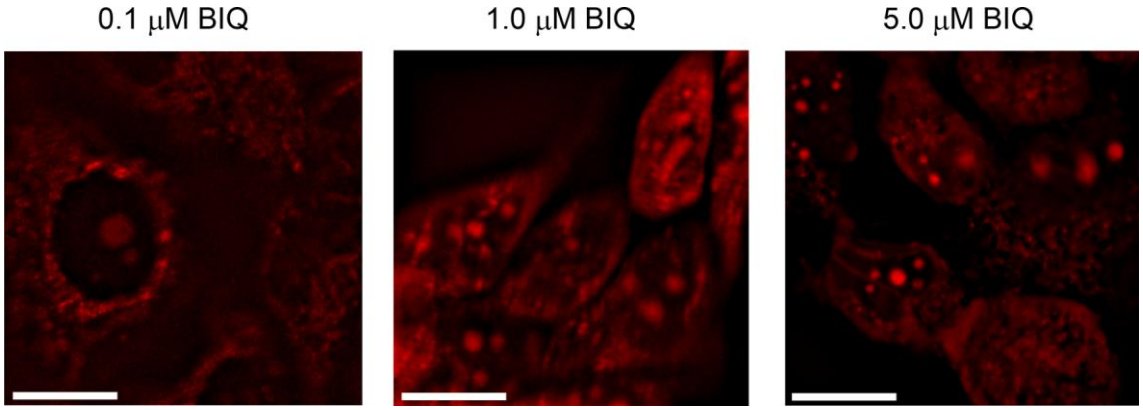

Figure S16. Fluorescence images of living MCF7 cells incubated with 0.1-5.0 μM BIQ for 24 h. Scale bar: 15 μm.

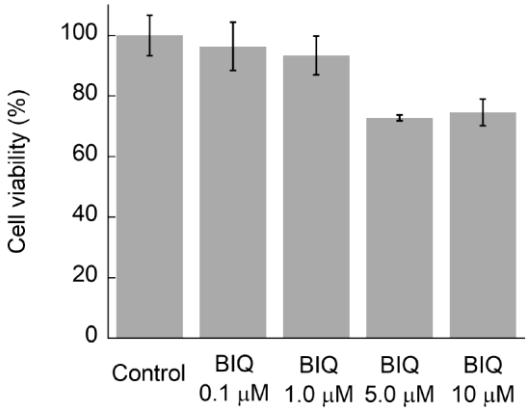

Figure S17. Evaluation of cytotoxicity of BIQ after 24 h incubation. Buffer treatment served as a positive control. Error bars represent standard deviation obtained from three independent experiments.

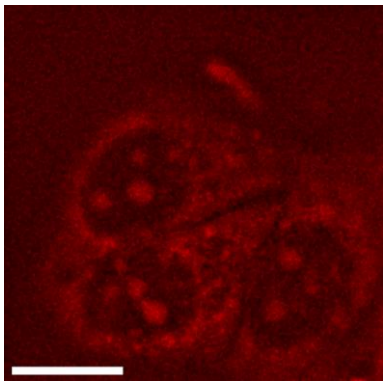

Figure S18. Fluorescence imaging of living MCF7 cells stained by BIQ with the no-wash protocol. Scale bar: 15 μm. Measurement conditions were the same as those given in Fig. 2A in the main text.

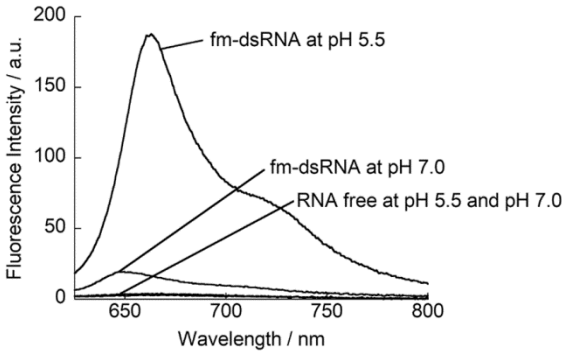

Figure S19. Fluorescence spectra of PNA-BIQ (1.0 μM) in the absence and presence of the fully-matched dsRNA (fm-dsRNA, 5.0 μM) at pH 5.5 or pH 7.0. Measurements were performed in a

10 mM sodium acetate buffer solution (pH 5.5) or a 10 mM sodium phosphate buffer solution (pH 7.0) containing 100 mM NaCl and 1.0 mM EDTA. Excitation, 611 nm. Analysis, 663 nm. Temperature, 25°C.

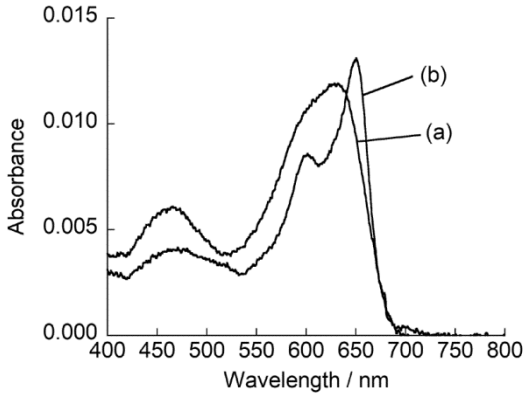

Figure S20. UV spectra of PNA-BIQ (1.0 μM) in the (a) absence and (b) presence of fm-dsRNA (1.0 μM). Other solution conditions were the same as those given in Fig. 4 in the main text.

The absorption band of the BIQ unit showed a red-shift with hyperchromicity upon binding to fm-dsRNA, as observed for the TO base surrogate (ref.22 in the main text). This indicates the intercalation of the BIQ unit into the triplex formed between PNA-BIQ and fm-dsRNA.

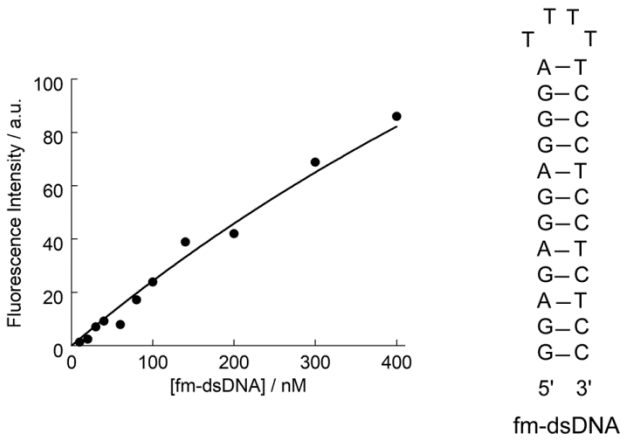

Figure S21. Fluorescence titration curve for the binding of PNA-BIQ for fm-dsDNA. [PNA-BIQ] = 50 nM. [fm-dsDNA] = 0-410 nM. Other solution conditions were the same as those given in Fig. 4 in the main text. The sequence of fm-dsDNA was also shown. Excitation, 611 nm. Analysis, 650 nm. Temperature, 25°C.

The dissociation constant (K_d) for fm-dsDNA was estimated as 1.5 μM. The affinity of PNA-BIQ for fm-dsDNA was two orders of magnitude weaker than that for fm-dsRNA, which strongly suggests the binding preference of PNA-BIQ for the dsRNA over the corresponding dsDNA.

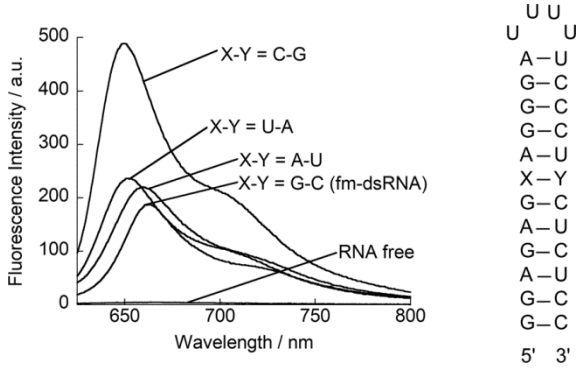

Figure S22. Effect of the base pair opposite the BIQ unit on the fluorescence response of PNA-BIQ. [PNA-BIQ] = 1.0 μM. [dsRNA] = 5.0 μM. Other solution conditions were the same as given in Fig. 4 in the main text. Excitation, 611 nm. Temperature, 25°C.

Table S1. Fluorescence quantum yield of PNA-BIQ, PNA-QB, and PNA-TO in the absence and presence of dsRNAs.[a]

	PNA-BIQ	PNA-QB[b]	PNA-TO[b]
RNA free	0.0026	0.0017	0.0028
X-Y =G-C	0.10	0.33	0.41
Y-Y = A-U	0.12	0.36	0.48
X-Y = C-G	0.23	0.029	0.083
X-Y = U-A	0.10	0.17	0.27

[a] [PNA-BIQ] = 1.0 μM, [dsRNA] = 1.0 μM. Other solution conditions were the same as given in Fig. 4 in the main text. [b] Values were from the literature (ref. 23 in the main text).

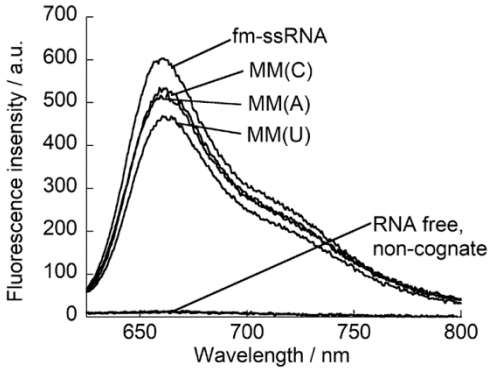

Figure S23. Fluorescence response of PNA-BIQ (1.0 μM) for target ssRNAs (1.0 μM): fully-matched (fm-ssRNA), single base mismatch-containing (MM(U), MM(A), MM(C)) and non-cognate sequence (5'-CCU GCU UUG CU-3'). Measurements were performed in a 10 mM sodium phosphate buffer solution (pH 7.0) containing 100 mM NaCl and 1.0 mM EDTA. Excitation, 611 nm. Temperature, 25°C.

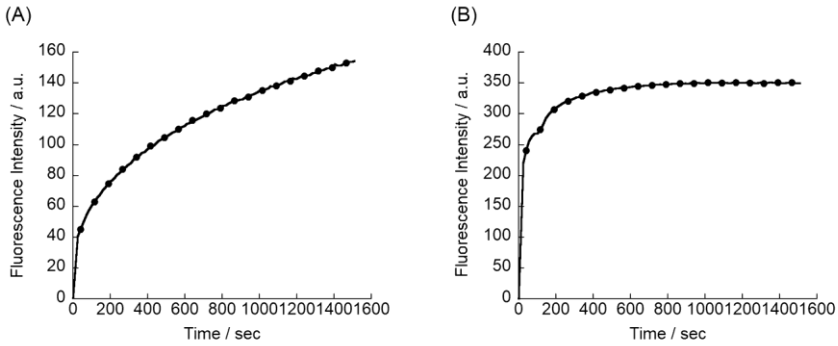

Figure S24. Time-dependent fluorescence change of the probes (5.0 μM: (A) BIQ and (B) SYTO RNA select) upon addition of 20 μM rG/rC. Other solution conditions were the same as those given in Fig. 1B in the main text. Excitation: 595 nm (BIQ); 490 nm (SYTO RNA select). Analysis: 645 nm (BIQ); 530 nm (SYTO RNA select). Temperature, 25°C.

Although both probes show the rapid increase in the fluorescence intensity upon addition of rG/rC, the response of SYTO RNA was found to be faster than that of BIQ. This indicates the slower binding kinetics of BIQ compared to SYTO RNA select.

References

(S1) Xue, X.; Zhang, Y.; Liu, Z.; Song, M.; Xing, Y.; Xiang, Q.; Wang, Z.; Tu, Z.; Zhou, Y.; Ding,

K.; Xu, Y. *J. Med. Chem.* **2016**, 59, 1565-1579.

(S2) Bethge, L.; Jarikote, D. V.; Seitz, O. *Bioorg. Med. Chem.* **2008**, 16, 114-125.

(S3) Joachimi, A.; Benz, A.; Hartig, J. S. *Bioorg. Med. Chem.* **2009**, 17, 6811-6815.

(S4) Sato, Y.; Kudo, M.; Toriyabe, Y.; Kuchitsu, S.; Wang, C-X.; Nishizawa, S.; Teramae, N. *Chem. Commun.* **2014**, 50, 515-517.